CHEMISTRY
A EUROPEAN JOURNAL

DOI: 10.1002/chem.200701644

Vesicles to Concentrate Iron in Low-Iron Media: An Attempt to Mimic Marine Siderophores

Lucie Bednarova,[a, c] Jérémy Brandel,[a] Amaury du Moulinet d'Hardemare,[a] Jan Bednar,[b] Guy Serratrice,*[a] and Jean-Louis Pierre*[a]

Abstract: Amphiphilic catechol-type iron chelators were studied with the aim of mimicking the properties of marine bacterial siderophores. The Fe^{III} complexation constants and aqueous solution speciation of L^{S10}, a sulfonated catechol unit that has a C_{10} lipophilic carbon chain connected by an amide linkage, were determined by spectrophotometric titration. The calculated value of pFe^{3+} is 18.1 at pH 7.4. Cryogenic transmission electron microscopy showed that the tris(catecholate) ferric complex formed at physiological pH initially assembles into micelles, in which the catecholate–iron units stay on the exterior of the micelle. The average diameter of these micelles was estimated to be 4.2 nm. The micelles then slowly rearrange into clusters of different sizes, which leads to the formation of unilamellar and bilamellar vesicles. The reorganization processes are comparable to those observed by Butler et al. for the marinobactin siderophores produced by marine bacteria, but in contrast to the marinobactins, vesicles of the Fe^{3+}–L^{S10} complex form without an excess of iron relative to ligand concentration. The time-dependent micelle-to-vesicle transition is discussed herein.

Keywords: iron · marine siderophore mimics · micelles · self-assembly · vesicles

Introduction

Although iron comprises about 5% of the Earth's crust, its availability to living organisms is limited as a result of its extremely low solubility under physiological conditions. Consequently, bacteria have evolved aggressive iron acquisition processes. Powerful and selective low-molecular-weight iron chelators (siderophores) are specifically produced and secreted in response to iron deficiency.[1] In contrast to the abundance of iron in terrestrial environments, iron concentrations in oceanic surface waters are low enough to limit the growth of photosynthetic marine microorganisms. It has been claimed in the iron hypothesis that an influx of iron into the oceans could promote the growth of phytoplankton and reduce atmospheric carbon dioxide levels. Butler et al. have evidenced a process in marine bacteria that promotes high local iron concentrations by using amphiphilic siderophores, which have polar peptidic head groups and hydrophobic fatty acid tails.[2] The amphiphilic surface-active nature of these siderophores leads to the formation of self-assembled structures.

We felt that a bioinspired study of this strategy might help in understanding the mechanism of iron uptake by organisms living in media with low iron concentrations, allow tuning of the hydrophilic/lipophilic balance of abiotic siderophores designed for iron nutrition,[3] and also provide a new strategy for the intricate problem of iron chelator delivery for the treatment of iron overload and related diseases[4] by reproducing the membrane affinity of the amphiphilic marinobactin siderophores.[5]

In a previous report we described the self-assembling properties and results of bacterial iron nutrition for simple

[a] Dr. L. Bednarova, Dr. J. Brandel, Dr. A. d. M. d'Hardemare, Prof. G. Serratrice, Prof. J.-L. Pierre
Université Joseph Fourier
Département de Chimie Moléculaire UMR-5250
ICMG FR-2607, CNRS, BP 53
38041, Grenoble Cedex 9 (France)
Fax: (+33)4-7651-4836
E-mail: Guy.Serratrice@ujf-grenoble.fr
Jean-Louis.Pierre@ujf-grenoble.fr

[b] Dr. J. Bednar
Université Joseph Fourier
Laboratoire de Spectrométrie Physique
UMR-5588, CNRS, BP 53
38041, Grenoble Cedex 9 (France)

[c] Dr. L. Bednarova
Institute of Organic Chemistry and Biochemistry
Academy of Sciences of the Czech Republic
Flemingovo 2, 166 10 Praha 6 (Czech Republic)

monodentate and tris(bidentate) synthetic catecholate Fe^{III} chelators.[6] We have also shown that the denticity of the ligand did not significantly influence the aggregation processes. These chelators and their Fe^{III} complexes have tensioactive properties, with a critical micelle concentration (CMC) of $<10^{-5}$ M at pH 7.4. The iron complexes self-assemble in solution at physiological pH values to form spherical particles (100–130 nm in diameter), whereas the free ligands are limited to micellar assembly. These ligands are good models for the physicochemical properties of siderophores from marine bacteria. Moreover, they have been shown to be effective in the iron nutrition of *Erwinia. chrysanthemi*. The poor water solubility of the free ligands and the formation of filled aggregates instead of the expected true vesicles led us to investigate sulfonated derivatives of the ligands previously studied. Sulfonation, which is often used by chemists to improve the water solubility of organic compounds (and particularly abiotic iron chelators), was not considered to be a biomimetic process until the recent discovery of a sulfonated metabolite of the catecholic siderophore petrobactin that was extracted from the oil-degrading marine bacterium *Marinobacter hydrocarbonoclasticus*.[7] Herein we present the self-assembling properties of the iron complex of sulfonated monocatechol derivative L^{S10} as opposed to unsulfonated ligand L^a previously studied.[6]

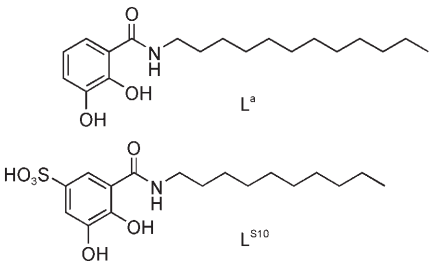

Results and discussion

Synthesis: Amphiphilic ligand L^{S10} was prepared by using a straightforward synthesis (Scheme 1). This method affords some advantages over the synthetic pathway previously described[6] because it avoids protection of the catechol moiety and the use of hydrolysable acyl chloride during the amidification step.

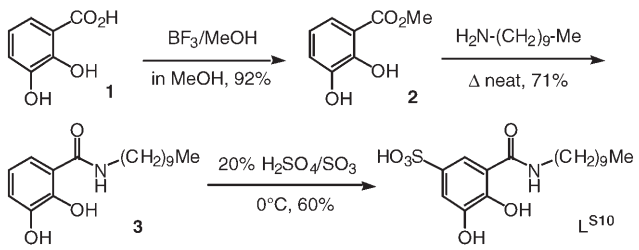

Scheme 1. The synthesis of L^{S10}.

First, 2,3-dihydroxybenzoic acid (**1**) was esterified with BF_3/MeOH, then ester **2** and decylamine were heated in the absence of a solvent to give amide **3**. Finally, sulfonation in 20% oleum gave L^{S10} in a satisfactory overall yield of 39%. The products were characterized by mass spectrometry and ^1H and ^{13}C NMR spectroscopies.

Ligand pK_a determination: The sulfonate group is a moderately strong acid (p$K_a<2$) and was considered to be deprotonated under our conditions. The deprotonation constants of the hydroxyl groups were determined by spectrophotometric titration according to the observed spectral changes between pH 3.5 and 10 (Figure 1; λ_{max} shifts from 302 to

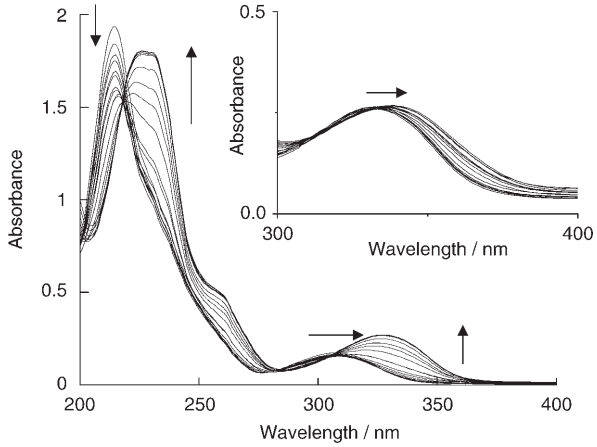

Figure 1. UV-visible absorption spectra of L^{S10} (1×10^{-4} M) recorded in water at pH 3.5 to 10 (main graph) and pH 10 to 12.5 (inset). Conditions: ionic strength $I=0.10$ M ($NaClO_4$); $T=(25.0\pm0.2)$ °C.

330 nm and 224 to 234 nm) and pH 10 and 12.5 (Figure 1, inset; λ_{max} shift from 330–339 nm). Analysis of the spectroscopic data by using the Specfit program[12] gave pK_a values of p$K_{a2}=(6.45\pm0.11)$ and p$K_{a1}=(11.9\pm0.2)$, as defined by Equations (1) and (2):

$$LH_n \rightleftharpoons LH_{n-1}+H^+ \quad (1)$$

$$K_{an}=\frac{[LH_{n-1}][H^+]}{[LH_n]} \quad (2)$$

The value of pK_{a2} is assigned to the *ortho*-hydroxyl proton, owing to the electron-withdrawing effect of the amide group. These pK_a values agree with those of 2,3-dihydroxy-5-sulfo-*N*,*N*-dimethylbenzamide (dmbs) and 2,3-dihydroxyterephtalamides derivatives.[8] The pK_{a2} value of the *ortho*-hydroxyl proton is significantly lower than the value of the unsulfonated analogue (p$K_a=9.07$), as a result of the electron-withdrawing effect of the sulfonate group.

Fe^{III} complex formation: The equilibria of the metal complexation process were studied by means of spectrophotometric titration. The spectra obtained from spectrophotometric titrations of the ferric complexes of L^{S10} are shown in

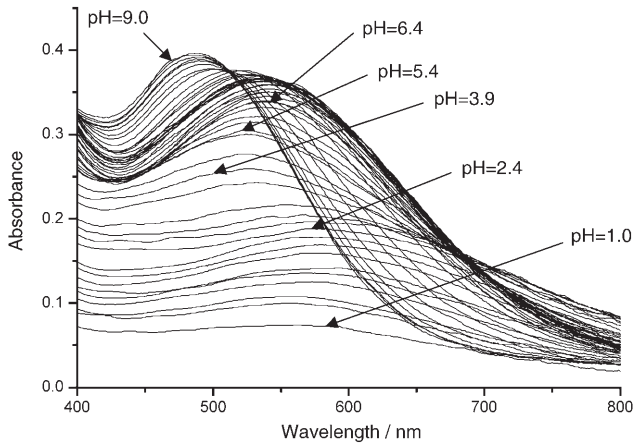

Figure 2. UV-visible absorption spectra of Fe^{3+}–L^{S10} ($[L^{S10}]_{tot}=3.0\times10^{-4}$ M, $[Fe^{3+}]=0.92\times10^{-4}$ M) in water as a function of pH. Conditions: $I=0.10$ M ($NaClO_4$), $T=(25.0\pm0.2)$ °C.

Figure 2. The absorbance data were refined with the Specfit program[12] and provided values for the global stability constants (β_{mlh}) of these ferric complexes. β_{mlh} is defined by Equations (3) and (4):

$$m\mathrm{Fe^{III}}+l\mathrm{L^{3-}}+h\mathrm{H^{+}} \rightleftharpoons \mathrm{Fe}_m\mathrm{L}_l\mathrm{H}_h \quad (3)$$

$$\beta_{mlh}=\frac{[\mathrm{Fe}_m\mathrm{L}_l\mathrm{H}_h]}{[\mathrm{Fe^{III}}]^m[\mathrm{L^{3-}}]^l[\mathrm{H^{+}}]^h} \quad (4)$$

in which m, l, and h are values in the general complex formula $[Fe_m(L^{S10})_lH_h]$ for these species.

By increasing the pH value from 1 to 9, a continuous increase in the absorbance was observed, and was accompanied by successive shifts in the value of λ_{max} (from $\lambda_{max}=$ 608 nm at pH 1–2.4 to 525, 550, 525, and 490 nm at pH ranges of 2.4–3.9, 3.9–5.4, 5.4–6.4, and 6.4–9.0, respectively). For the spectral shift from 608-490 nm an isosbestic point was observed at $\lambda=514$ nm. In an analysis of the spectroscopic data, considering the formation of $[FeL^{S10}H]^+$, $[Fe(L^{S10})_2H_2]^-$, $[Fe(L^{S10})_3H_3]^{3-}$, $[Fe(L^{S10})_3H]^{5-}$ and $[Fe(L^{S10})_3]^{6-}$ species gave the best fit. The values of $\log\beta_{mlh}$ are presented in Table 1 and the calculated spectra and species distribution diagram are shown in Figure 3. The protonated species are related to a salicylate mode of coordination that involves the oxygen atoms of the carboxyl and *ortho*-hydroxyl groups. The spectral characteristics of the $[Fe(L^{S10})_3H_3]^{3-}$, $[Fe(L^{S10})_3H]^{5-}$ and $[Fe(L^{S10})_3]^{6-}$ species indicate a change from a tris(salicylate) to a tris(catecholate) coordination. However, note that the value of $\lambda_{max}=510$ nm for $[Fe(L^{S10})_2H_2]^-$ is very low and should be higher than the value for $[Fe(L^{S10})_3H_3]^{3-}$.

Table 1. Equilibrium constants ($\log\beta_{mlh}$) and UV-visible spectral characteristics of complexes with the general formula $[Fe_m(L^{S10})_lH_h]$.[a]

	$\log\beta_{mlh}$	ε [$M^{-1}cm^{-1}$]	λ [nm]
$[FeL^{S10}H]^+$	20.3 ± 0.1	2700	630
$[Fe(L^{S10})_2H_2]^-$	39.6 ± 0.2	3500	510
$[Fe(L^{S10})_3H_3]^{3-}$	58.3 ± 0.2	3900	560
$[Fe(L^{S10})_3H_1]^{5-}$	48.3 ± 0.1	4000	550
$[Fe(L^{S10})_3]^{6-}$	40.6 ± 0.2	4400	490

[a] Solvent: water, $I=0.10$ M ($NaClO_4$), $T=25.0$ °C

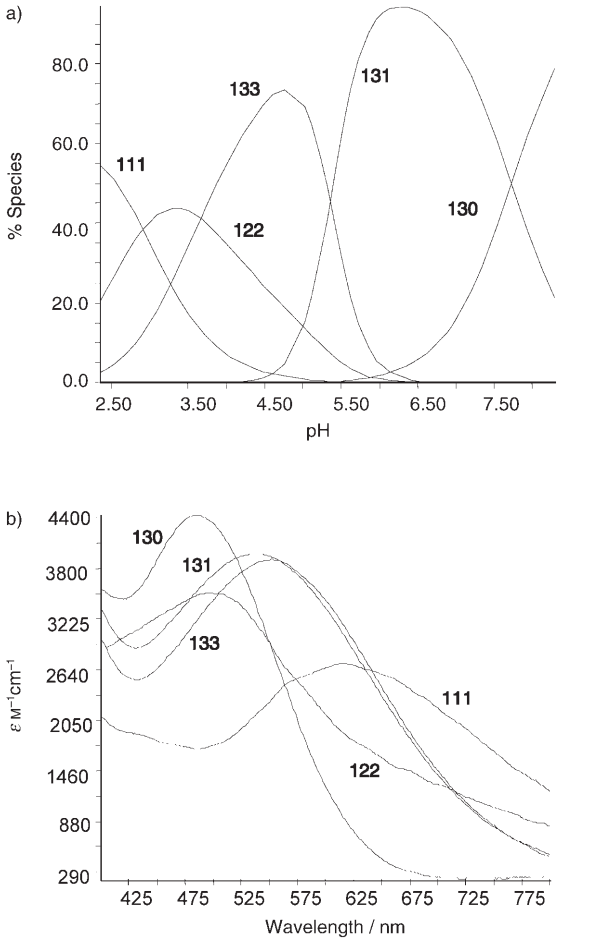

Figure 3. a) Species distribution diagram of $[Fe_m(L^{S10})_lH_h]$ as a function of pH. b) Calculated absorption spectra for all $[Fe_m(L^{S10})_lH_h]$ species present in solution ($[L^{S10}]_{tot}=3.36\times10^{-4}$ M, $[Fe^{3+}]=1.12\times10^{-4}$ M). The three-digit labels on each graph give values for m, l, and h.

The stoichiometry of the ferric complex at pH 7.4 was also studied by monitoring the charge-transfer absorption band at $\lambda=490$ nm in aqueous solution (Figure 4). The titration curve of absorbance versus [Fe]/[L] (Figure 4) exhibits a plateau for [Fe]/[L] > 0.3, which clearly confirms the formation of a complex that contains three ligand molecules and one ferric cation. In comparison, the unsulfonated analogue forms a bis(chelate) complex at pH 7.4 and a tris(chelate) at a pH of around 9.[6] This can be attributed to the high pK_a value of the *ortho* hydroxyl, which does not allow the coordination of a third bidentate unit at neutral pH.

The value of $pFe^{3+}=-\log[Fe^{3+}]$ for $[Fe^{3+}]_{tot}=10^{-6}$ M and $[L]_{tot}=10^{-5}$ M has been calculated to be 18.1 at a physiological pH value of 7.4. This value is comparable to the pFe^{3+} value of 19.2 calculated for the dmbs ligand.[8a]

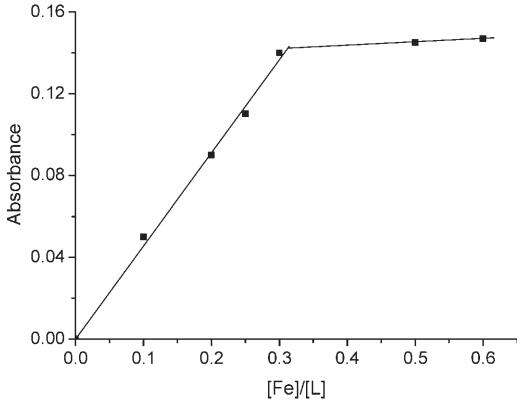

Figure 4. The absorbance at $\lambda = 490$ nm as a function of the molar ratio $[Fe^{3+}]/[L]$ ($[L^{S10}]_{tot} = 1 \times 10^{-4}$ M). Conditions: 3-(*N*-morpholino)propanesulfonic acid (MOPS) buffer (0.05 M), pH 7.4, $T = (25.0 \pm 0.2)$ °C.

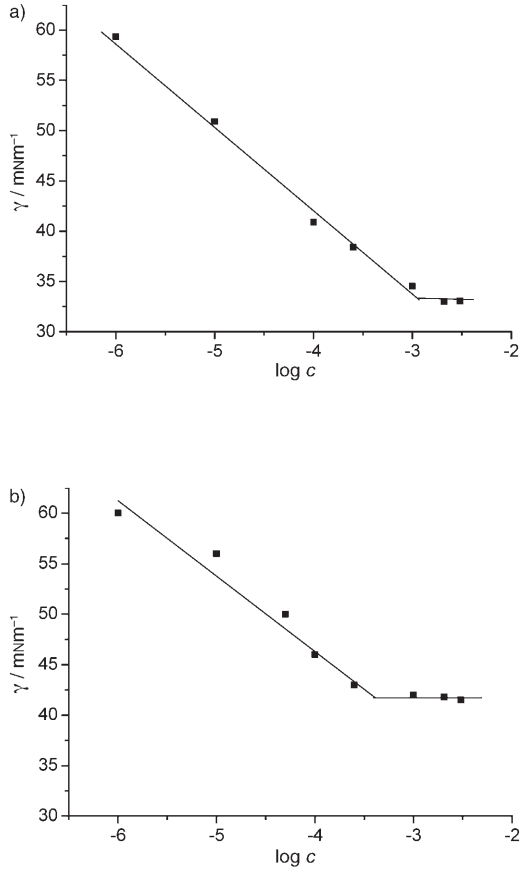

Figure 5. a) Dependence of the surface tension on $[L^{S10}]_{tot}$ (1×10^{-6}–3×10^{-3} M). b) Dependence of the surface tension on the concentration of the Fe^{3+}–L^{S10} complex ($[Fe^{3+}]_{tot} = 1 \times 10^{-6}$–$3 \times 10^{-3}$ M; $[L^{S10}]_{tot}/[Fe^{3+}] = 3{:}1$). Conditions: MOPS buffer (0.05 M), pH 7.4, $T = (25.0 \pm 0.2)$ °C.

CMC determination and dynamic light scattering (DLS) studies: The CMC values of L^{S10} and its ferric complex were determined from surface tension measurements at pH 7.4 (Figure 5).

The CMC value of the free ligand (1.2 mM) is in agreement with those of similar molecules.[9] The CMC of the ferric complex was found to be 0.45 mM, which is lower than the CMC of the free ligand. This could be owing to the higher hydrophobicity of the complex, which contains three ligand molecules, and therefore, three hydrocarbon tails. Note that this CMC is significantly higher than that of the siderophores produced by marine bacteria (e.g., marinobactins), which have CMC values of 50–75 μM.[2a]

The DLS experiments allowed us to estimate the micellar size of L^{S10} and its Fe^{III} complex under our experimental conditions. The results for the free ligand at pH 7.4 show that the molecules spontaneously self-organize into particles with one size distribution of around 5(1) nm and another that ranges from 30 to 70 nm (polydispersity index = 0.56(3)), which suggests that these micelles tend to form large aggregates. The results from measurements of solutions of the Fe^{III} complex revealed two distributions of particles sizes, which were centered around 4.0(5) and 50(5) nm (polydispersity index = 0.52(4)). The first size distribution at around 4 nm can be ascribed to the self-organization of the Fe^{3+}–L^{S10} molecules into micelles. Interestingly, this average distribution suggests that the Fe^{III} complexes form smaller micelles than the free ligand. This confirms that our model behaves in an analogous way to the natural siderophore Marinobacter E,[2] and can be explained by the fact that coordination of iron makes the headgroup bigger, which results in a larger headgroup/tail volume ratio and leads to the formation of smaller micelles. The second size distribution at around 50 nm could be ascribed to the presence of vesicles and/or aggregated micelles. The high polydispersity of all of our samples reveals many different structures, which include micelles, micellar aggregates of different shapes and sizes, and vesicles. These micellar aggregates might intermediates in the formation of vesicles. This assumption was confirmed by analysis of the same solution in the presence of octanol (1% (v/v)). A unique, monodisperse distribution at 60(10) nm (polydispersity index = 0.23(1)) was observed. These results are in good agreement with the different structures observed in the cryogenic transmission electron microscopy (cryo-TEM) images (Figure 6).

Cryo-TEM studies: We used cryo-TEM to visualize the assemblies of the Fe^{3+}–L^{S10} complex at pH 7.4. The ratio of the ligand and Fe^{3+} concentrations ($[L^{S10}]/[Fe^{3+}]$) was 3:1. The microscopy was performed 8 h and 8 d after preparation of the complex (Figure 6).

Figure 6a shows micelles with an average diameter of 4.2 nm, which is in good agreement with the estimated size of the ferric complex (≈ 2 nm). The sharp increase in contrast on the periphery of the micelles indicates that the hydrophilic heads, which contain the complexed Fe^{III} cations, are located on the outside of the micelles as expected. However, a time-dependent reorganization occurs and the micelles tend to aggregate into clusterlike structures. Cryo-TEM images recorded 8 d after specimen preparation showed a variety of structures that included a few isolated

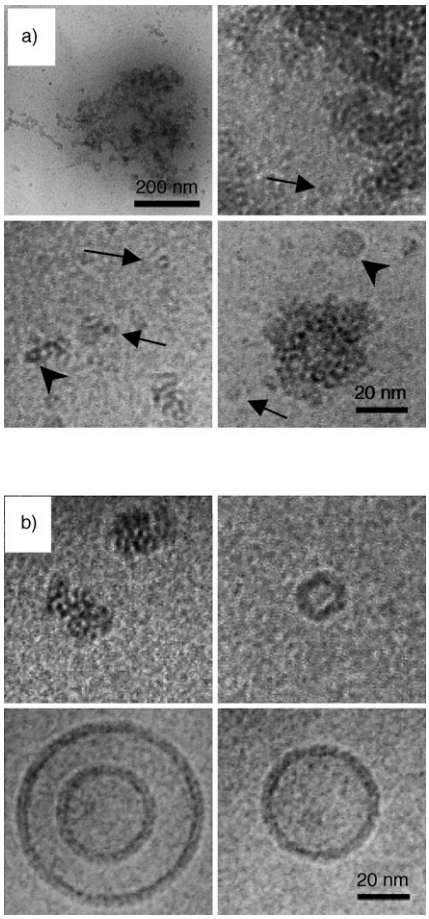

Figure 6. Cryo-TEM micrographs of Fe^{3+}–L^{S10} ($[L^{S10}]_{tot}=2.5$ mM, $[Fe^{3+}]_{tot}=0.83$ mM), recorded 8 h (a) and 8 d (b) after sample preparation. Conditions: MOPS buffer (0.05 M), pH 7.4. The arrows indicate micelles and the arrowheads indicate clusterlike structures. Unless otherwise indicated all images were recorded on the 20 mm scale.

micelles identical to those observed after 8 h, some clusters with rather random or spherical shapes, and many unilamellar vesicles that apparently originate from the fusion of micelles (Figure 6b). The thickness of the bilayer was identical to the micelle diameter, which suggests that the vesicles are formed from a bilayer of ferric complex molecules that arise from micelle fusion. Upon the addition of octanol (1% v/v, 6.10^{-3} M), vesicle formation was observed only 8 h after preparation of the sample. The morphology of these vesicles, and particularly their layer thickness, was identical to those previously observed for Fe^{3+}–L^{S10} only (Figure 7). Few micelles with an average diameter of 4.2 nm were observed after 8 h (Figure 7, inset), in contrast to the results for Fe^{3+}–L^{S10} only after the same time interval.

It is interesting to compare these new results to those previously published for the unsulfonated analogue L^a.[6] The results for L^a were obtained in the presence of methanol (5% v/v) owing to the very low solubility of the ferric complex. Neither micelles nor vesicles were observed, but spherical aggregates around 100 to 300 nm in size were formed, an example of which is depicted in Figure 8a. The image of

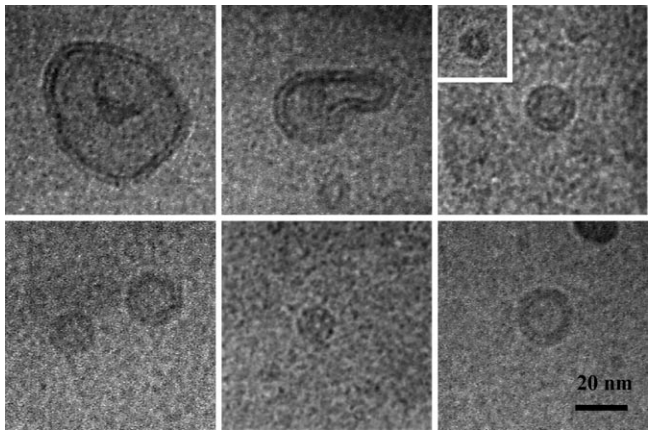

Figure 7. Cryo-TEM micrographs of Fe^{3+}–L^{S10} ($[L^{S10}]_{tot}=2.5$ mM, $[Fe^{3+}]_{tot}=0.83$ mM) in the presence of octanol, taken 8 h after sample preparation. Conditions: MOPS buffer (0.05 M), pH 7.4, octanol (1% v/v; added to the ferric complex immediately after preparation). Inset: a micelle with average diameter of 4.2 nm.

the particle reveals some bilayer structures near the surface, but insufficient contrast does not allow the space between the bilayers to be clearly resolved. Power analysis of the image was performed by fast Fourier transform, and indicated a periodic structure with a repeat distance of ≈4 nm (Figure 8b). This strongly suggests that the spherical aggregates are bilayered multilamellar vesicles around 4 nm in bilayer diameter, which is in agreement with the length of the

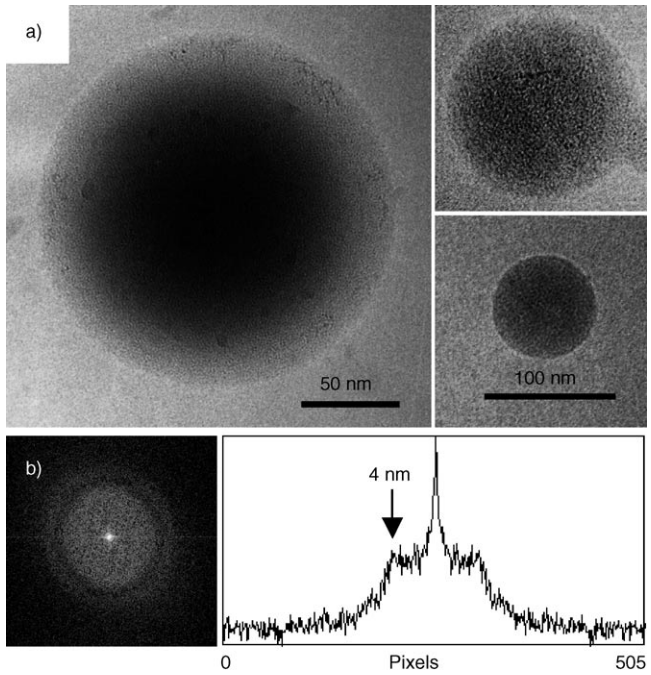

Figure 8. a) Cryo-TEM micrographs of Fe^{3+}–L^a ($[L^a]_{tot}/[Fe^{3+}]=2:1$). Conditions: MOPS buffer (0.05 M), pH 7.4, methanol (5% v/v), octanol (1% v/v). b) A power spectrum obtained by fast Fourier transformation of the original image (left) and its profile. The arrow indicates the repeat distance of ≈4 nm.

complex molecule and very close to the size of the micelles observed with L^{S10}.

The iron complex of L^a forms the species $[Fe(L^aH)_2]^+$ at pH 7.4, which differs significantly from the ferric complex of L^{S10} in charge and stoichiometry. For the L^a complex, the polar head group is weakly positively charged and the hydrophobic part contains only two carbon chains. As a consequence, the repulsive force between the polar heads of the unilamellar bilayers is weak and the formation of multilamellar vesicles is favored. In contrast, ligand L^{S10} forms a mixture of highly charged $[Fe(L^{S10})_3]^{6-}$ and $[Fe(L^{S10})_3H]^{5-}$ species at pH 7.4. At first, they assemble into spherical micelles as expected, then transform into unilamellar vesicles as shown in Figure 6. The cone-shaped aggregation mode responsible for micelle formation with free L^{S10} at pH 7.4 (polar head $[L^{S10}]^{3-}$ and one hydrophobic carbon chain) changes to a truncated cone-shape aggregation mode after iron complex formation. In this case, the hydrophilic head is large and strongly charged and the hydrophobic tail of the complex is formed by three carbon chains, which favors a vesicular rearrangement. The micelle-to-vesicle transition was relatively slow, which could be a result of the spatial rearrangement of the hydrophobic carbon chains in the octahedral coordination geometry of the ferric complex. In the presence of octanol (1% v/v), the micelle-to-vesicle transition was significantly faster (Figure 7). It is assumed that the octanol molecules penetrate into the surface of the micelle and reduce the electrostatic repulsion between the negatively charged head groups. This favors a low-curvature vesicle structure and thus accelerates the formation of vesicles.

Conclusion

The ferric complex of the amphiphilic catechol bidentate ligand L^{S10} allowed us to illustrate the transformation from micelles to vesicles upon Fe^{III} coordination, as described for marine siderophores by Butler et al.[2] Like marinobactins, free L^{S10} self-assembles into micelles. After formation of the iron complex, micelles are observed first, followed by a slow transition into vesicles. Nevertheless, there are some differences between marine siderophores and L^{S10}. The formation of ferric complexes of the tripodal (tris(bidentate)) marine siderophores is connected to the folding of the siderophore, that is, the shift in the apo-form structure of the siderophore towards the creation of an "iron pocket". Moreover, the charge of the apo-marinobactin does not change upon Fe^{III} complexation.[2d] In contrast, Fe^{III} complexation by the monopodal catechol ligand L^{S10} implies the formation of a 3:1 $[L]/[Fe^{3+}]$ species and a change in charge upon complex formation. These differences should strongly influence the kinetics of micelle formation and the micelle-to-vesicle transition. Furthermore, it should be emphasized that vesicle formation with marine siderophores is observed in the presence of an excess of iron with respect to the ligand, in contrast to the monopodal catecholate L^{S10}. The micelle-to-vesicle transition is dependent not only on the amphiphilic properties of the molecules studied and their changes after iron complexation, but also on the type and flexibility of the hydrophilic, chelating part of the molecule. Our study reveals that simple ligands, such as L^{S10} and L^a, may serve as models to mimic the strategy of phytoplankton to concentrate Fe^{III} into vesicles.

To estimate the influence of these vesicles in digestive processes, the metabolic processes of the bacterium *E. chrysanthemi* (see Ref. [6]) are currently being studied. The syntheses of ligands that contain a fluorescent group to help visualize the iron chelation process and the transport of iron across membranes are in progress, as is a study of the membrane affinity of L^{S10}.

Experimental Section

Reagents: Stock solutions of Fe^{III} for titrations were prepared by dissolving appropriate amounts of ferric perchlorate hydrate (Aldrich) in standardized solutions of $HClO_4$ (Argos) or $NaClO_4$ (Prolabo Puriss) in water. The solutions were standardized for Fe^{3+} ions spectrophotometrically by using a molar extinction coefficient of $4160\,M^{-1}cm^{-1}$ at 240 nm in an aqueous solution of $HClO_4$ (0.1 M).[10] A fresh stock solution of ferric perchlorate hydrate (2.5×10^{-2} M) was prepared for each experiment.

Synthesis of L^{S10}

*Methyl-2,3-dihydroxybenzoate (**2**)*: A solution of BF_3 in methanol (15 mL) was added to a solution of **1** (5.07 g, 32.8 mmol) in anhydrous methanol (100 mL) and the mixture was heated at reflux for 4 h. The volatile compounds were removed under vacuum and cold water (200 mL) was added. The mixture was then adjusted to pH 6 with 4 M aqueous sodium hydroxide and extracted with CH_2Cl_2 (3×25 mL). The resulting organic phase was dried over Na_2SO_4 and concentrated under vacuum to give **2** as a pink solid that was sufficiently pure for the next step (5.11 g, 92%). M.p. = 79 °C; ^{1}H NMR (200 MHz, $CDCl_3$, 18 °C): $\delta = 3.93$ (s, 3H; OCH_3), 5.88 (s, 16H; OH, intramolecularly bonded), 6.77 (t, $^3J(H,H) = 7.8$ Hz, 1H), 7.10 (dd, $^3J(H,H) = 7.8$, $^4J(H,H) = 1$ Hz, 1H), 7.33 (dd, $^3J(H,H) = 7.8$, $^4J(H,H) = 1$ Hz, 1H), 10.90 ppm (s, 1H; OH).

*N-decyl-2,3-dihydroxybenzamide (**3**)*: A mixture of **2** (2.20 g, 13 mmol) and decylamine (2.06 g, 13 mmol) was heated under argon at 110 °C for 24 h. The residue was then dissolved in Et_2O (100 mL) and the organic phase was washed with water (2×15 mL) and brine (2×15 mL), dried over Na_2SO_4, and concentrated under vacuum. The resulting dark oil was purified by flash chromatography (silica gel) with hexane/dichloromethane (gradient 60:40 to 10:90) as the eluent to give **3** as a pink waxy solid (2.74 g, 71%). ^{1}H NMR (300 MHz, $CDCl_3$, 18 °C): $\delta = 0.88$ (t, $^3J(H,H) = 6.6$ Hz, 3H; CH_3), 1.18–1.56 (m, 14H; CH_2), 1.61 (q, $^3J(H,H) = 6.6$ Hz, 2H), 3.44 (t, $^3J(H,H) = 6.6$ Hz, 2H; CH_2N), 5.85 (s, 1H; OH, intramolecularly bonded), 6.35 (s, 1H; NH), 6.73 (t, $^3J(H,H) = 7.8$ Hz, 1H), 6.7 (dd, $^3J(H,H) = 7.8$, $^4J(H,H) = 1.4$ Hz, 1H), 7.33 (dd, $^3J(H,H) = 7.8$, $^4J(H,H) = 1.4$ Hz, 1H), 12.78 ppm (s, 1H; OH); ^{13}C NMR (75 MHz, $CDCl_3$, 18 °C): $\delta = 14.1$ (CH_3), 22.6, 26.9, 29.2, 29.4 and 29.5 (CH_2), 31.8 (CH_2CH_2N), 39.8 (CH_2N), 114.1 ($C_{q\,arom}$), 115.8, 117.9 and 118.5 (CH_{arom}), 146.0 and 149.1 ($C_{q\,arom}$), 169.9 ppm (C=O); MS (DCI, NH_3/iC_4H_{10}): m/z (%): 294 (100) $[M+H]^+$; elemental analysis calcd (%) for $C_{17}H_{27}NO_3$: C 69.59, H 9.28, N 4.77; found: C 69.68, H 9.29, N 4.72.

3-decylcarbamoyl-4,5-dihydroxybenzene-sulfonic acid (L^{S10}): Compound **3** (1.3 g, 4.4 mmol) was added portionwise to oleum (20%, 20 mL) at 0 °C. The mixture was kept at room temperature for 12 h before ice (10 g) was carefully added. The residue was diluted with methanol (100 mL) and the volatile compounds were removed under vacuum. The oil obtained was carefully triturated in CH_2Cl_2 (3×20 mL) and Et_2O (2×10 mL) and the solvents were discarded. The residual solvents were evaporated in vacuo to give L^{S10} as a highly hygroscopic semisolid (0.99 g, 60%). ^{1}H NMR (300 MHz, CD_3OD, 18 °C): $\delta = 0.87$ (t, $^3J(H,H) = 6.5$ Hz, 3H; CH_3), 1.23–1.45 (m, 14H; CH_2), 1.61 (q, $^3J(H,H) = 6.5$ Hz, 2H), 3.38 (t, $^3J(H,H) =$

7 Hz, 2H; CH_2N), 7.36 (d, ^4J(H,H) = 2 Hz, 1H), 7.68 ppm (d, ^4J(H,H) = 2 Hz, 1H); ^{13}C NMR (75 MHz, CD_3OD, 18 °C): δ = 15.2 (CH_3), 24.5, 28.8, 31.0, 31.2 and 31.4 (CH_2), 33.8 (CH_2CH_2N), 41.7 (CH_2N), 117.0 ($C_{q\,arom}$), 117.7 and 117.9 (CH_{arom}), 137.1, 148.1 and 152.6 ($C_{q\,arom}$), 171.5 ppm (C=O); MS (DCI, NH_3/iC_4H_{10}): m/z (%): 374 (100) $[M+H]^+$; elemental analysis calcd (%) for $C_{17}H_{27}NO_6S\cdot H_2O$: C 52.16, H 7.47, N 3.58; found: C 52.08, H 7.51, N 3.52.

Spectrophotometric studies: The solutions were prepared with boiled deionised water, which was deoxygenated and flushed continuously with argon (purified by a Sigma Oxiclear cartridge) to exclude CO_2 and O_2. An ionic strength of 0.1 M was maintained with $NaClO_4$ (Prolabo, Puriss or Merck, p.a.) and all measurements were carried out at (25.0 ± 0.2) °C. The free hydrogen concentrations were measured with a glass-Ag/AgCl combined electrode (Metrohm or Tacussel High Alkalinity, filled with 0.1 M aqueous NaCl and saturated with AgCl). The electrode was calibrated to measure [H] by the classical method of titrating $HClO_4$ (0.01 M) with NaOH (0.02 M).[11] Spectrophotometric measurements were carried out by using a Varian Cary 50 UV/Vis spectrophotometer equipped with a Peltier thermostatting accessory and a PC for data collection and evaluation. The spectrophotometric titrations were recorded in aqueous solutions with an ionic strength of 0.1 M (adjusted with 0.1 M aqueous $NaClO_4$ for L^{S10} or $NaClO_4$+$HClO_4$ for the complex) at 25 °C between pH 3.5 and 12.6 for L^{S10} (1.0×10^{-4} M) and between pH 1 and 10 for the ferric complex (ligand = 3.36×10^{-4} M, $Fe^{3+} = 1.0\times10^{-4}$ M). The pH was adjusted with NaOH. The stoichiometry of the Fe^{III} complex at pH 7.4 was also monitored by titrating a solution of ligand with a solution of Fe^{III} in a buffer solution (MOPS = 0.05 M, $NaClO_4$ = 0.05 M).

The spectrophotometric data were processed with the SPECFIT/32 Global Analysis system (Spectrum Software Associates).[12] This program performs a global analysis of system equilibria, and by using a nonlinear regression model given by the Levenberg–Marquardt method we can calculate the thermodynamic constants and spectra of absorbing species. Calculating the protonation constants of the ligand was achieved by using two spectral sets. For pK_{a2}, readings were taken between pH 2 and 8 in the 200 to 400 nm spectral region with a 1 nm step, and for pK_{a1}, readings were taken between pH 8 and 12.6 in the 300 to 400 nm spectral region with a 1 nm step. Calculating the complexation stability constant was achieved by using the spectral set of the iron complex between pH 1 and 10 in the 400 to 800 nm spectral region with a 1 nm step.

Surface tension studies: The surface tension was measured at 25 °C by using an automatic drop tensiometer (Tracker, I.C. Concept, Longessange France) in rising drop mode. The surface tension was calculated by a mathematical analysis of the axial symmetric shape of the drop (Laplacian profile). The CMC was estimated from the change in surface tension due to the concentrations of the ligand (1×10^{-6}–3×10^{-3} M) and complex (3×10^{-7} M–1×10^{-3} M; $[Fe^{3+}]_{tot}/[L^{S10}]_{tot}$ = 1:3). All experiments were performed at 25 °C in a buffer solution (MOPS, 0.05 M, pH 7.4).

DLS studies: DLS measurements were performed by using a Zetasizer Nano Series ZS (Malvern Instruments) instrument equipped with a 633 nm laser. The non-invasive back-scatter detection method was used in which the incident beam does not have to pass through the sample, but instead the light scattered 173° from the incident beam was measured. Data were fitted by using Dispersion Technology Software v5.00 (DTS; Malvern Instruments). The DTS software uses algorithms to extract the decay rates of the correlation function for a range of particle sizes. This information is then used to produce a size distribution of the hydrodynamic diameter. The basic intensity distribution is obtained from the DLS measurements, from which all other distributions are generated by using Mie theory. The results are presented as an estimate of the size distribution of the most numerous particles. Experiments were performed in buffer solution (MOPS, 0.05 M, pH 7.4) for the ligand (2×10^{-3} M) and the ferric complex (1×10^{-3} M) at 25 °C. The solutions were passed through a filter (Pall, Acrodisc CR 13 mm Syringe Filter with a 0.45 μm PTFE Membrane) prior to analysis to exclude dust particles.
Cryo-TEM studies: Experiments were performed with the ferric complexes of L^a and L^{S10}. Samples of the ferric complex of L^{S10} ($[L^{S10}]_{tot} = 5\times10^{-4}$ M, $[Fe^{3+}]_{tot} = 0.83\times10^{-3}$ M) were prepared in buffer solution (MOPS, 0.05 M, pH 7.4) in the absence and presence of octanol (1% v/v, 6×10^{-3} M). Samples of the ferric complex of L^a ($[L^a]_{tot} = 5\times10^{-4}$ M, $[Fe^{3+}]_{tot} = 2.5\times10^{-4}$ M) were prepared in buffer solution (MOPS, 0.05 M, pH 7.4) with methanol (5% v/v) and also with octanol (1% v/v, 6×10^{-3} M). The samples were prepared 8 h before the first experiment and the second experiment was performed on the samples 8 d later. The samples for cryo-TEM were prepared by the following procedure:[13] a 3 μL drop of the sample solution was applied to a grid covered with a holey carbon/Pt-carbon film, the excess liquid was blotted with Whatman 40 filter paper, and the remaining film was vitrified in liquid ethane held just above freezing point. The grid was then mounted in a Gatan 626 cryoholder (Gatan, Pleasanton CA) and observed at −180 °C with a Philips CM200 electron microscope operating at 80 kV. Micrographs were recorded in low-dose mode on Kodak SO-163 film (Eastman Kodak, Rochester NY) at a direct magnification of 50000× and ≈1 μm defocus, and developed in full-strength D19 developer (Kodak) for 12 min. Contrast enhancements and intensity gradient removal of the images were performed with Scion Image software.

Acknowledgements

We gratefully acknowledge Professors Marguerite Rinaudo and Michel Milas for help in performing the surface tension measurements in their laboratory, Dr. Anabelle Varrot for assistance with the scattering measurements (Centre de Recherches sur les Macromolécules Végétales (CERMAV-UPR CNRS 5301, Grenoble), and Gisèle Gellon for the synthesis of L^{S10}.

[1] J. B. Neilands, *J. Biol. Chem.* **1995**, *270*, 26723–26726.
[2] a) J. S. Martinez, G. P. Zhang, P. D. Holt, H. T. Jung, C. J. Carrano, M. G. Haygood, A. Butler, *Science* **2000**, *287*, 1245–1247; b) K. Barbeau, E. L. Rue, K. W. Bruland, A. Butler, *Nature* **2001**, *413*, 409–412; c) A. Butler, *Biometals* **2005**, *18*, 369–374; d) T. Owen, R. Pynn, J. S. Martinez, A. Butler, *Langmuir* **2005**, *21*, 12109–12114.
[3] a) D. Imbert, P. Baret, D. Gaude, I. Gautier-Luneau, G. Gellon, F. Thomas, G. Serratrice, J.-L. Pierre, *Chem. Eur. J.* **2002**, *8*, 1091–1100; b) L. Yun-Ming, M. J. Miller, U. Möllmann, *Biometals* **2001**, *14*, 153–157; c) J. I. Wirgau, A. L. Crumbliss, *Inorg. Chem.* **2003**, *42*, 5762–5770.
[4] D. Z. Liu, R. C. Hider, *Medicinal Research Reviews* **2002**, *22*, 26–64
[5] a) J. S. Martinez, J. N. Carter-Franklin, E. L. Mann, J. D. Martin, M. G. Haygood, A. Butler, *Proc. Natl. Acad. Sci. USA* **2003**, *100*, 3754–3759; b) G. Xu, J. S. Martinez, J. T. Groves, A. Butler, *J. Am. Chem. Soc.* **2002**, *124*, 13408–13415; c) J. D. Martin, Y. Ito, V. V. Homann, M. G. Haygwood, A. Butler, *J. Biol. Inorg. Chem.* **2006**, *11*, 633–641
[6] M. Apostol, P. Baret, G. Serratrice, J. Desbrieres, J.-L. Putaux, M.-J. Stebe, D. Expert, J.-L. Pierre, *Angew. Chem.* **2005**, *117*, 2636–2638; *Angew. Chem. Int. Ed.* **2005**, *44*, 2580–2582.
[7] S. J. H. Hickford, F. C. Kupper, G. Zhang, C. J. Carrano, J. W. Blunt, A. Butler, *J. Nat. Prod.* **2004**, *67*, 1897–1899.
[8] a) W. R. Harris, K. N. Raymond, F. L. Weitl, *J. Am. Chem. Soc.* **1981**, *103*, 2667–2675; b) T. M. Garett, P. W. Miller, K. N. Raymond, *Inorg. Chem.* **1989**, *28*, 128–133.
[9] P. D. T. Huibers, V. S. Lobanov, A. R. Katritzky, D. O. Shah, M. Karelson, *J. Colloid Interface Sci.* **1997**, *187*, 113–120.
[10] R. Bastian, R. Weberling, F. Palilla, *Anal. Chem.* **1956**, *28*, 459–462.
[11] A. E. Martell, R. J. Motekaitis, *Determination and Use of Stability Constants*, VCH, Weinheim, **1988**, Chapter 1, pp. 7–19.
[12] a) H. Gampp, M. Maeder, C. J. Meyer, A. D. Zuberbühler, *Talanta* **1985**, *32*, 95–101; b) H. Gampp, M. Maeder, C. J. Meyer, A. D. Zuberbühler, *Talanta* **1985**, *32*, 257–264.
[13] J. Dubochet, M. Adrian, J. J. Chang, J. C. Homo, J. Lepault, A. W. McDowall, P. Schultz, *Q. Rev. Biophys.* **1988**, *21*, 129–228.

Received: October 17, 2007
Published online: February 21, 2008

